Volume 1 | Number 1 | Jan 2013 | Pages 1–100

Dalton Transactions

An international journal of inorganic chemistry
www.rsc.org/dalton

ROYAL SOCIETY OF CHEMISTRY

This is an *Accepted Manuscript*, which has been through the Royal Society of Chemistry peer review process and has been accepted for publication.

Accepted Manuscripts are published online shortly after acceptance, before technical editing, formatting and proof reading. Using this free service, authors can make their results available to the community, in citable form, before we publish the edited article. We will replace this *Accepted Manuscript* with the edited and formatted *Advance Article* as soon as it is available.

You can find more information about *Accepted Manuscripts* in the **Information for Authors**.

Graphical Abstract

A newly designed and structurally characterised rhodamine based Schiff base (**L**) which can sense nanomolar level of Al^{3+} ions through CHEF process and its Al(III) complex (**L′-Al**) behaves as a highly F^- ions selective chemosensor through fluorescence quenching in HEPES buffer (1 mM, pH 7.4; EtOH / water: 1/3, v/v) at 25 °C. Interestingly the non-cytotoxic Al^{3+} ion selective **L** and F^- ion selective complex **2** are highly potential biomarkers to recognize the intercellular distribution of respective ions in living cells under fluorescence microscope.
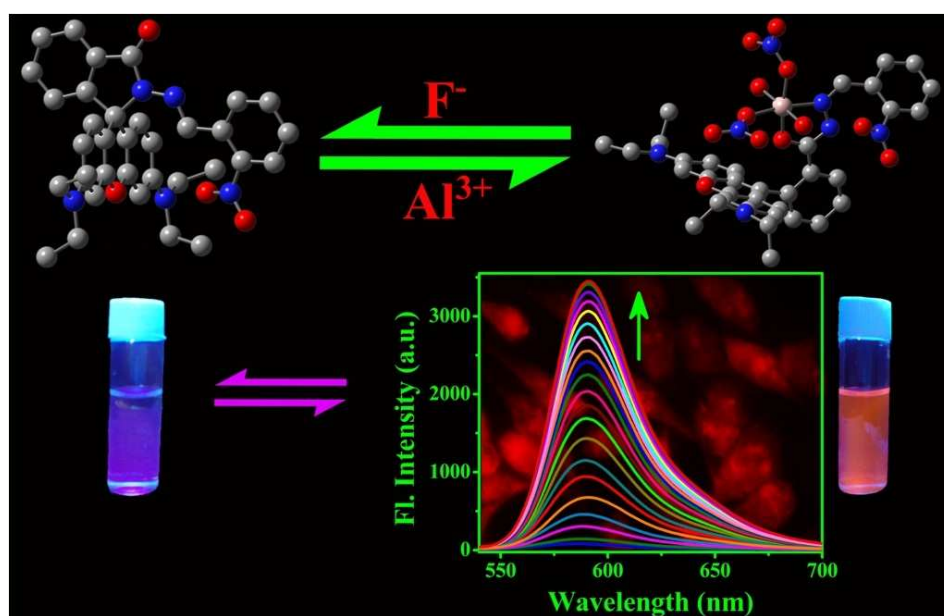
ARTICLE TYPE

A rhodamine based 'turn-on' Al^{3+} ion selective reporter and resultant complex as secondary sensor of F$^-$ ion applicable in living cell staining†

Buddhadeb Sen,[a] Manjira Mukherjee,[a] Samya Banerjee,[b] Siddhartha Pal[a] and Pabitra Chattopadhyay*,[a]

A newly designed fluorescent aluminium(III) complex (**L′-Al** / **2**) of structurally characterised non-fluorescent rhodamine based Schiff base (**L**) was isolated in pure form, and characterised by detailed spectroscopic and physico-chemical tools along with the theoretical (DFT) supports. On addition of Al(III) ions to the solution of **L** in HEPES buffer (1 mM, pH 7.4; EtOH / water: 1/3, v/v) at 25 °C, the
10 systematic enhancement of fluorescence through chelation enhanced fluorescence (CHEF) process enables to detect the Al(III) ions as low as 60 nM with high selectivity, which was not affected by the presence of the competitive ions. Interestingly Al(III) complex (**L′-Al** / **2**) can specifically detect fluoride ions through quenching of the fluorescence in the presence of a huge amount of other anions in HEPES buffer (1 mM, pH 7.4) at 25 °C. On the basis of thorough experimental and theoretical findings, the
15 additions of Al^{3+} ions to the solution of **L** helps to generate a new fluorescence peak at 590 nm due to the selective binding of Al^{3+} ions with **L** in a 1 : 1 ratio with a binding constant (K) of 8.13 x 10^4 M^{-1}. Moreover, **L** showed no cytotoxic effect and it could be employed for the identification of intracellular concentration of Al^{3+} ions and F$^-$ ions by **2** in living cells under a fluorescence microscope.

Introduction

20 The design, synthesis and spectroscopic characterization of novel fluorescent chemosensor are of current interest and attracting much attention from the viewpoint of biomimmetic chemistry.[1] Development of various fluorescent artificial receptors that are able to transform the binding of ionic species into spectroscopic
25 signals has expanded rapidly due to the simplicity, high sensitivity and real-time monitoring with a low response time of fluorescence spectroscopy.[2] The fluorescence lifetime and quantum yield are perhaps the most important characteristics of a fluorophore. In this context, rhodamine is a class of dyes with
30 long-wavelength absorption and emission, high absorption coefficient and quantum efficiency, and good photostability. It is widely available and used in industrial coloration, biomarkers, and fluorometric probes.[3-5]

These 'recognition and signaling" molecules may also
35 stimulate the investigation of molecular sensors for biologically relevant aluminium ions which are widely used in our daily lives, often as pharmaceuticals, packaging material and cooking utensils,[6] in the paper industry,[7] in dye production,[8] in the textile industry,[9] as a component of many cosmetic preparations and
40 aluminium salts are currently utilized in alimentary industry.[10] Aluminium chlorohydrate (ACH) is a water-soluble aluminium complex which is the active ingredient in some antiperspirants.[11] Apart from this, the toxicity of aluminum endangers the aquatic life and influences agricultural production in acidic soils.[12-13]
45 Aluminum salts are neurotoxic and are suspected to induce Parkinson's disease,[14] Alzheimer's disease,[15] microcytic anemia, dialysis dementia, osteomalacia and even to risk the cancer of lung and bladder.[16-18] The FAO/ WHO Joint Expert Committee on Food Additives recommend a maximum daily intake of
50 aluminium of 3-10 mg per day body mass. Determination of Al^{3+} is highly challenging also for its poor coordination ability, strong hydration ability and lack of favorable spectroscopic characteristics.[19]

In recent years the field of anion recognition has also grown
55 exponentially due to the significant role of anions in environmental, biological and industrial systems.[20-25] Anion recognition with metal complexes has an advantage as they furnish electrostatic interactions that can authenticate anion binding even in semi-aqueous / aqueous medium. Moreover,
60 recently we encourage to design those metal complexes which upon coordination with another analyte (usually anion), changes the fluorescence signature of metal complex in favor of sensing and recognition of the target analyte. The smallest anion, fluoride, with high charge density is of particular importance because of its
65 roles in dental care and other areas like it is a common component in drugs and cockroach poisons.[26-27] Fluoride induces cavity formation as well as discoloration of teeth. A fluoride concentration above 1.5 ppm carry an increasing risk of dental fluorosis, and much higher concentrations lead to skeletal
70 fluorosis resulting in severe joint pain, thyroid activity depression, bone disorders and can affect the immune system.[28-30]

Although there are several chemosensors for only Al^{3+} ions[31] or only F$^-$ ions[32] in literature but the fluorosensors for both Al^{3+} and F$^-$ ions are scarce.[33] Again, the sensors for both the ions
75 suffer from tedious synthesis procedure, low sensitivity or slow

response, turn-off fluorescence response, poor water solubility and interferences from other ions.

Herein, we report a newly designed and structurally characterised rhodamine based Schiff base (**L**) which can sense nanomolar level of Al^{3+} ions through chelation enhanced fluorescence (CHEF) process and its Al(III) complex (**L′-Al**) behaves as a highly F^- ions selective chemosensor through quenching of the fluorescence in HEPES buffer (1 mM, pH 7.4; EtOH / water: 1/3, v/v) at 25 °C. The competitive ions do not affect the selectivity and specificity of this probe towards the detection of Al^{3+} and F^- ions. Interestingly this non-cytotoxic probe (**L**) is also helpful for the detection of intracellular Al^{3+} ions or F^- ions concentrations by **2** under a fluorescence microscope. Compared to the previous reports, this easy to synthesized probe behaves as a Al^{3+} ion selective sensor as low as nanomolar region in bio-friendly semi-aqueous solvent-medium with both excitation and emission wave lengths in the visible range of more significant in the field of development of chemosensor of biological relevant ions.[31] Moreover, here the sensing process is reversible and the probe could be recycled for further use.[33] Besides, "OFF-ON-OFF" fluorescence behavior observed in the presence of Al^{3+} and F^- ions strengthens the potential applications of the **L′-Al** complex as a device with '**INHIBIT**' logic gate functions.[31g]

Experimental section

Synthesis of the probe (L)

The probe (**L**) was synthesised by the following procedure (Scheme 1). At first, the rhodamine B-hydrazide (**1**) was prepared following a literature method.[34] In the second step *o-nitrobenzaldehyde* (136 mg, 1.0 mmol) was dissolved in ethanol and was added to the ethanolic solution rhodamine-B hydrazide (456 mg, 1.0 mmol) with stirring. Then the resulting solution was reflux for 4 h. Evaporated to a small volume and cooled, white colored crystalline product obtained which was filtered out and then recrystallized from pure methanol. Single crystals were obtained from this solution, one of which was selected for doing the crystallographic study. Yield: 76 %, mp (^oC): 217 ± 2.

L. $C_{35}H_{35}N_5O_4$: Anal. Found: C, 71.05; H, 5.91; N, 11.96; Calc.: C, 71.29; H, 5.98; N, 11.88. IR (cm^{-1}): ν_{NH} = 3446; $\nu_{C=C(aromatic)}$ = 2972; $\nu_{C=O}$ = 1695; $\nu_{CH=N}$ = 1614. ^{1}HNMR (500 MHz, DMSO-d_6): 9.019 (s, 1H, CH=N); 7.925 (t, 2H); 7.78 (d, 1H); 7.694-7.651 (m, 1H); 7.629 (d, 1H); 7. 571 (q, 2H); 7.101 (d, 1H); 6.426 (d, 2H); 6.401(s, 2H); 6.333 (d, 2H); 3.27 (q, 8H, 4CH$_2$); 1.058 (t, 12H, 4CH$_3$). ^{13}CNMR (DMSO-d_6): 165.128, 153.482, 152.202, 149.484, 149.137, 141.538, 135.305, 134.461, 131.655, 129.868, 129.470, 128.998, 128.403, 127.682, 125.547, 124.827, 124.132, 109.059, 105.756, 98.481, 66.424, 44.622, 13.235. ESI-MS (in ethanol): $[M + H]^+$, m/z, 590.2736 (100 %) (calcd.: m/z, 590.2769; where M = molecular weight of **L**].

Synthesis of L′-Al complex (2)

To a 10 mL ethanolic solution of **L** (0.1 mmol, 59 mg), a solution of aluminium nitrate (0.1 mmol, 38 mg) was added dropwise and stirred for 4 h. Solvent was reduced to a small volume using a rotary evaporator, and kept in a beaker to get the crystalline blood red solid on slow evaporation (Scheme 1). The pure solid was collected by filtration followed by washing with cold methanol-

water, and then dried in vacuo for performing the analytical work.

[Al(L′)(NO₃)₂(H₂O)₂].(NO₃): $C_{35}H_{39}AlN_8O_{15}$: Anal. Found: C, 49.99; H, 4.61; N, 13.45; Calc.: C, 50.12; H, 4.69; N, 13.36. IR (cm^{-1}): ν_{NH} = 3454; $\nu_{C=C(aromatic)}$ = 2974; $\nu_{CH=N}$ = 1616; $\nu_{N-O(NO3,sym)}$, 1383. ^{1}HNMR (500 MHz, DMSO-d_6): 8.999 (s, 1H, CH=N); 7.925 (t, 2H); 7.779 (d, 1H); 7.700-7.654 (m, 1H); 7.633 (d, 1H); 7.574 (q, 2H); 7.102 (d, 1H); 6.427 (d, 2H); 6.400(s, 2H); 6.336 (d, 2H); 3.264 (q, 8H, 4CH$_2$); 1.059 (t, 12H, 4CH$_3$). ^{13}CNMR (DMSO-d_6): 165.512, 153.484, 152.209, 149.488, 149.141, 141.536, 135.708, 135.307, 134.468, 131.661, 129.878, 129.473, 128.986, 128.406, 127.685, 125.549, 124.832, 124.127, 109.056, 105.759, 98.485, 44.612, and 13.236. ESI-MS (in ethanol): $[M + H]^+$, m/z, 776. 2486 (10 %) (calcd.: m/z, 776.2467; where M = molecular weight of **L**].

X-Ray crystallography

X-ray data of the suitable crystal of **L** was collected on a Bruker's Apex-II CCD diffractometer using MoKα (λ = 0.71073). The data were corrected for Lorentz and polarization effects and empirical absorption corrections were applied using SADABS from Bruker. A total of 22055 reflections were measured out of which 5359 were independent and 3974 were observed [I > 2σ(I)] for theta (θ) 1.33 to 25.03°. The structure was solved by direct methods using SIR-92 and refined by full-matrix least squares refinement methods based on F^2, using SHELX-97.[35] All calculations were performed using Wingx package.[36,37] Important crystallographic parameters are given in Table S1†. The crystallographic data of **L** have been deposited to Cambridge Crystallographic Data Centre bearing the CCDC no. of 997189.
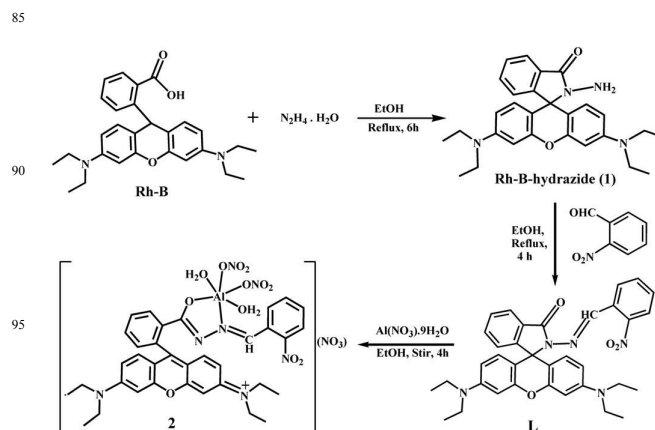
Scheme 1 Synthetic strategy of **L** and **L′-Al** complex

General method of UV-vis and fluorescence titration

For UV-vis and fluorescence titrations, stock solution of **L** was prepared in HEPES buffer (1 mM, pH 7.4; 25% EtOH) at 25 °C. Fluorescence measurements were performed using 5 nm x 5 nm slit width. All the fluorescence and absorbance spectra were taken after 10 minutes of mixing to get the optimized spectra.

Theoretical calculation

To clarify the understanding of the ground state configurations of the **L** and the corresponding complex (**2**) DFT calculations were performed using Gaussian-09 software over a Red Hat Linux IBM cluster. Molecular level interactions have also been studied using density functional theory (DFT) with the B3LYP/6-31G (d,

p) functional model and basis set.[38] Vertical electronic excitations based on B3LYP optimized geometry was computed using the time-dependent density functional theory (TD-DFT)[39] formalism in water using conductor-like polarizable continuum model (CPCM)[40] was used to calculate the fractional contributions of various groups to each molecular orbital. The lowest 20 singlet states along the vertical excitation energies are computed here.

Preparation of cell and *in vitro* cellular imaging with L

Human cervical cancer cell, HeLa and breast cancer cell (MCF-7) cell line was purchased from National Center for Cell Science (NCCS), Pune, India and was used throughout the study. Cell were cultured in Dulbecco's modified Eagle's medium (DMEM, Gibco BRL) supplemented with 10% FBS (Gibco BRL), and 1% antibiotic mixture containing penicillin, streptomycin and neomycin (PSN, Gibco BRL), at 37 °C in a humidified incubator with 5% CO_2. For experimental study, cells were grown to 80-90 % confluence, harvested with 0.025 % trypsin (Gibco BRL) and 0.52 mM EDTA (Gibco BRL) in PBS (phosphate-buffered saline, Sigma Diagnostics) and plated at desire cell concentration and allowed to re-equilibrate for 24h before any treatment. Cells were rinsed with PBS and incubated with DMEM-containing L (10 μM, 1% DMSO) for 30 min at 37 °C. All experiments were conducted in DMEM containing 10% FBS and 1% PSN antibiotic. The imaging system was composed of a fluorescence microscope (ZEISS Axioskop 2 plus) with an objective lens [10×].

Cell cytotoxicity assay

To test the cytotoxicity of L, MTT [*3-(4,5-dimethyl-thiazol-2-yl)-2,S-diphenyl tetrazolium bromide*] assay was performed with the help of the literature procedure.[41] After treatments of the probe (50, 25, 12.5, 6.25, 3.12, 1.56, 0.78 μM), 10μl of MTT solution (10mg/ml PBS) was added in each well of a 96-well culture plate and incubated continuously at 37°C for 6 h. All mediums were removed from the wells and replaced with 100μl of acidic isopropanol. The intracellular formazan crystals (blue-violet) formed were solubilized with 0.04 N acidic isopropanol and the absorbance of the solution was measured at 595 nm wavelength with a microplate reader. Values are means ± S.D. of three independent experiments. The cytotoxicity of L was calculated as a percentage of cell viability and expressed in terms of IC_{50}.

Fluorescence microscopy

HeLa and MCF-7 cells (4 x 10^4 cells / mm^2), plated on cover slips, and were incubated with 10 μM of of L for 30 min. After washing with 50 mM phosphate buffer, pH 7.4 containing 150 mM NaCl (PBS), required volumes of $Al(NO_3)_3$ stock solution in DMSO were added such that final conc. of $Al(NO_3)_3$ adjusted to 5, 7 and 10 μM (DMSO will be 1%) and incubated for 30 min. After washing with PBS, mounted in 90% glycerol solution containing Mowiol, an anti-fade reagent, and sealed. Images were acquired using Apotome.2 fluorescence microscope (Carl Zeiss, Germany) using an oil immersion lens at 63 X magnification. The images were analyzed using the Axio Vision Rel 4.8.2 (Carl Zeiss, Germany) software.[41c] Fluorescence images were taken using the excitation wave length 530 nm. After taking images again we have incubated the cells with 50 μM NaF for 30 min and images were taken following the above procedure.

Result and discussion

Synthesis and structural characterisation

The synthesis of L involves at first the conversion of rhodamine B to rhodamine B-hydrazide which was allowed to react with *ortho nitrobenzaldehyde* at 1:1 mole ratio in dry ethanol (Scheme 1). The probe, L was characterised by physico-chemical and spectroscopic tools (Figs. S1-S4†). In the FTIR spectrum of L, the bands for CH=N, C=O and NH groups at 1614, 1695 and 3446 cm^{-1}, respectively along with other characteristic peaks (*viz.* Fig. S1, ESI†) were obtained. The QTOF-ESI+ spectrum of L showed the molecular ion peak at m/z 590.2736 corresponding to [L+H$^+$] (Fig. S2, ESI†). The well-resolved ^{1}H NMR and ^{13}CNMR spectra of L are in support of the formulation and the structure established by single crystal X-ray crystallographic analysis. Single crystals of the probe (L) were obtained from the pure methanolic solution. The crystal structure reveal the spiro lactam configuration (spiro atom, C_{15}) with the metal chelating residue orthogonal to the oxo-tricyclic ring system of the rhodamine moiety, which conformation makes the probe non-fluorescent. The L crystallizes in the triclinic space group P$\bar{1}$. An molecular view of the probe with atom labelling scheme is illustrated in Fig. 1, and a selection of bond distances and angles are listed in Table S2†.

The red colored L′-Al complex (2) was obtained by adding the solution of aluminium nitrate to an ethanolic solution of L in equimolar ratio with stirring for 4 h (Scheme 1). The ESI mass spectrum of 2 in ethanol exhibited a molecular-ion peak at m/z 776.2486 with ~10% abundance assignable to the formulation of 2 as [**Al(L′)(NO$_3$)$_2$(H$_2$O)$_2$**]$^+$ (calculated value at m/z, 776.2467). A characteristic peak for $v_{N-O(NO3,sym)}$ at 1383 cm^{-1} in the FTIR spectrum of 2 confirms the existence of nitrate anion. The characteristic signals for the corresponding proton and the carbon atoms of L were acquired in the ^{1}HNMR and ^{13}CNMR spectra of 2 in DMSO-d$_6$, which confirms the presence of the L bound to Al^{3+} ions (Figs. S5-S8†).
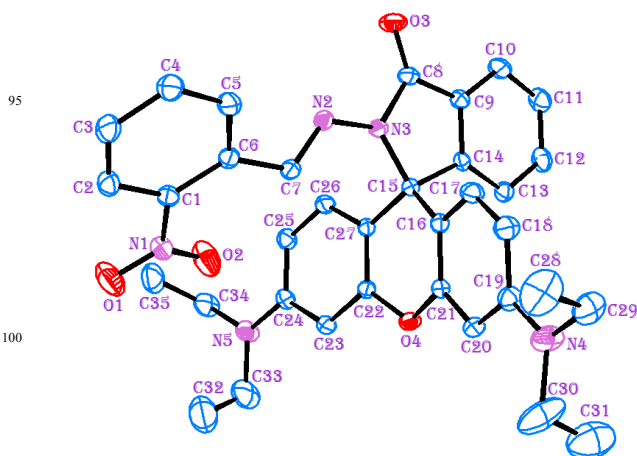
Fig. 1 An ORTEP view of L (30% probability) with atom numbering scheme (H atoms are omitted for clarity).

UV-Vis spectroscopic studies

UV-Vis spectra of L was recorded in HEPES buffer (1 mM, pH 7.4; 25% ethanol) at 25 °C showed an absorption at 312 nm

which may possibly be attributed to the intramolecular charge transfer transition. On incremental addition of Al^{3+} ions (0-20 μM) a new absorption peak at *ca.*566 nm along with a shoulder at *ca.*527 nm gradually developed due to the formation of **L'-Al** complex indicated by the visual color change from colourless to pink (Fig. 2).

On account of the complexity of the intracellular environment, an additional examination of the probe was performed to determine whether other ions were potential interferents or not. To establish this fact, metal ion selectivity assays were performed while keeping the other experimental condition unchanged. No significant change in the UV-vis spectral pattern was observed upon the addition of 10 equivalents excess of relevant metal ions *i.e.* Na^+, K^+, Ca^{2+}, Mg^{2+}, Cr^{3+}, Mn^{2+}, Fe^{3+}, Co^{2+}, Ni^{2+}, Zn^{2+}, Cd^{2+}, Hg^{2+}, and Pb^{2+}.
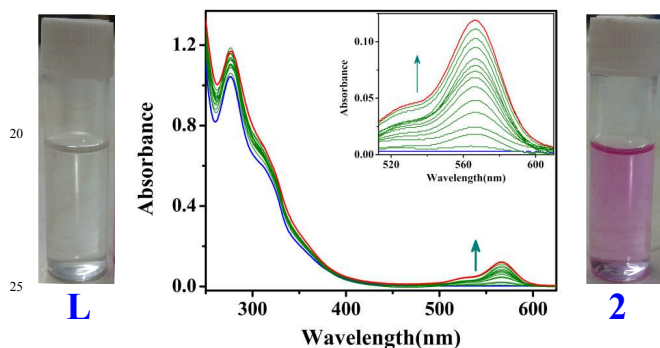
Fig. 2 UV-vis titration spectra of **L** (10 μM) upon incremental addition of Al^{3+} ions (0-20 μM) with naked eye visual color change of **L** only and **L'-Al** complex (**2**) in HEPES buffer (1 mM, EtOH / water: 1/3, v/v; pH 7.4) at 25 °C.

Effect of pH

To optimize the pH of the experimental condition, a pH study has been performed to control the efficiency of the probe (**L**). In absence of Al^{3+} ions, the probe, **L** exhibited weak fluorescence and showed pH independency over the pH range 6.0-10.0 (Fig. S9†). At low pH the probe showed high emission intensity due to the fact that at low pH the spirolactam ring opens irrespective of metal ions added.[42] However, it was noticed that the presence of Al^{3+} ions enhances selectively the emission intensity of **L** significantly at pH 6.0-10.0.

Fluorescence studies of L

On excitation at 525 nm, the probe, **L** exhibits very weak emission intensity at 590 nm as the closed spirolactum ring didn't show any emission.[42] On addition of various concentrations of Al^{3+} ions (0-20 μM), fluorescence intensity at 590 nm was increased significantly and systematically by a near about ~42-fold (Fig. 3). The fluorescence quantum yield has also been calculated in absence and presence of Al^{3+} ions and from this measurement it is clear that the fluorescence quantum yield in presence of Al^{3+} ions (Φ = 0.51) increases ~25 times than that of free **L** (Φ = 0.02). This spectral feature for the addition of Al^{3+} ions was evidenced by the fluorescence colour change from colourless to orange red in presence of UV light.

Selectivity

The fluorescence response of the organic moiety toward the

different metal ions was investigated with 50 times concentrations of alkali and alkaline earth metal ions (Na^+, K^+, Ca^{2+}, Mg^{2+}), transition (Cr^{3+}, Mn^{2+}, Fe^{3+}, Co^{2+}, Ni^{2+}, Cu^{2+}, Zn^{2+}, Cd^{2+}, Hg^{2+}) and some other metal ions (Al^{3+}, Pb^{2+}) (Fig. S10†). It reveals that the organic moiety has an excellent selectivity and specificity towards Al^{3+} ions over the other cations verified by the fluorescence color change from colourless to orange red in presence of UV light (Fig. S11†). In presence of 10 times excess of various tested ions together with **L** and Al^{3+} ions, almost no adverse effect on intensity was observed (Fig. S12†). Interestingly, the introduction of other metal ions causes the fluorescence intensity to be either unchanged or weakened.
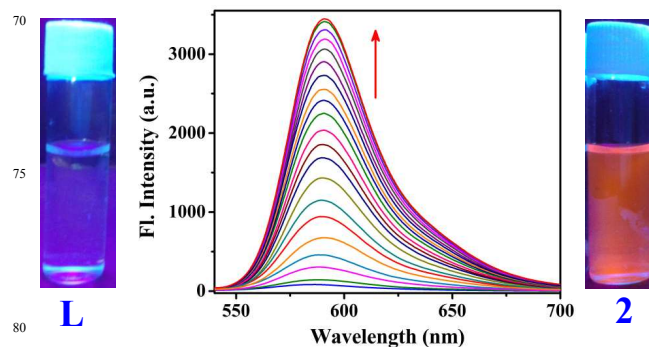
Fig. 3 Emission spectra of **L** (10 μM) in presence of Al^{3+} ions (0-20 μM) at λ_{ex} = 525 nm with naked eye fluorescence color change **L** only and **L'-Al** complex (**2**), in HEPES buffer (1 mM, EtOH / water: 1/3, v/v; pH 7.4) at 25 °C.

Job's plot from fluorescence experiments

A series of solution containing **L** and Al^{3+} ions were prepared such that the total concentration of **L** remained constant (10 μM) in all the sets. The mole fractions of Al^{3+} ions were varied from 0.1 to 0.7. The fluorescence intensity (**L**) at 590 nm was plotted against mole fraction $[Al^{3+}]$ ions. From Job's plot analysis (Fig. S13†) it is revealed that maximum emission shows at 1:1 ratio. These data indicate that the complex species in solution should form 1:1 complex with Al^{3+} ions in accordance with the mass and NMR spectral observations.

Binding constant calculation

The binding constant value was determined from the emission intensity data following the modified Benesi-Hildebrand equation.[43,44]

$$1/(F_x-F_0)=1/(F_{max}-F_0)+(1/K\,[C])(1/(F_{max}-F_0)$$

where F_0, F_x, and F_{max} are the emission intensities of probe, **L** considered in the absence of Al^{3+} ions, at an intermediate Al^{3+} ions concentration, and at a concentration of complete interaction, respectively, and where K is the association constant and [C] is the Al^{3+} ions concentration. K value (8.13 x 10^4 M^{-1} for **L**) was calculated from the intercept / slope using the plot of $(F_{max} - F_0)/(F_x-F_0)$ against $[C]^{-1}$ (Fig. S14†). From the value of K, it is reflected that **L** has a stronger binding affinity towards the Al^{3+} ions.

Detection limit calculation

To calculate the detection limit the calibration curve (Fig. S15†) in the lower region were drawn. From the slope of the curve (S)

and the standard deviation of seven replicate measurements of the zero level (σ_{zero}) the detection limit was estimated using the equation $3\sigma/S$.[45] This study indicates that the detection limit of **L** for Al^{3+} ions was found to be 60.37 nM.

NMR study

To ensure the formation of the **L′-Al** complex **(2)** in solution state, ^1H NMR titration was also performed in DMSO-d_6 from which it can be said that the addition of Al^{3+} ions caused the shifting of some characteristic peaks into the downfield (H_h, H_i), broadening of some peak (H_k) and shortening of the singlet peak for the imine hydrogen (H_l, at δ = 9.01 ppm in **L**) with upfield shifting (at δ = 8.99 ppm in **L′-Al** complex), but the peaks corresponding to the other hydrogens of the benzene and xanthene did not show any significant change (Fig. S16†). The formation of **L′-Al** species through usual ring opening has also been ascertained by performing the $^{13}CNMR$ experiment of **L** in absence and presence of Al^{3+} ions, from which it was observed that the signal at δ = 66.424 ppm attributable to the tertiary carbon (sp^3-hybridized) of the spiro-lactam ring in **L** (C_{15}) was absent in the spectrum of **L′-Al** complex (Figs. S3, S7, ESI†).[31b]

TCSPC Experiment

In the fluorescence average life time measurement the life time of **L** was found to be 0.15 ns at λ_{em}= 590 nm. After addition of Al^{3+} ions to the solution of **L**, the average lifetime of the **L′-Al** complex (at λ_{em}= 590 nm) increased to 1.04 ns (**L** : Al^{3+} ; 1 : 1), and it is clearly ascribed by the chelation enhanced fluorescence (CHEF) process (Fig. 6, Table S3†). The strong binding of Al^{3+} ions with organic moiety (**L**), is evidenced by the significant binding constant value (8.13 x 10^4 M^{-1}) and this phenomenon played a key role to deter the PET process in support of the selective detection of Al^{3+} ions through fluorescence enhancement (Scheme 2).
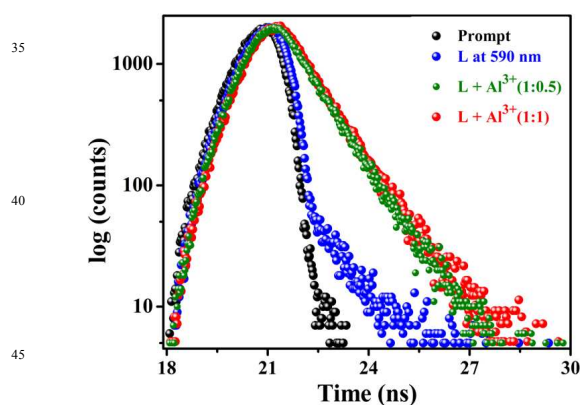
Fig. 4. Time resolved fluorescence decay of **L** (10μM) only and in presence of added Al^{3+} ions in HEPES buffer (1 mM, pH 7.4) at 25 °C using a nano LED of 550 nm as the light source at λ_{em} = 590 nm.

According to the equations:[46] τ^{-1} = k_r + k_{nr} and k_r = Φ_f/τ, the radiative rate constant k_r and total nonradiative rate constant k_{nr} of organic moiety, **L** and Al^{3+} complex with **L** were listed in Table S3†. The data suggest that k_r /k_{nr} ratio has been enhanced due to the reasonable decrease of k_{nr} in support of fluorescent enhancement of the **L′-Al** complex attributable to CHEF process.

Geometry optimization

To clarify the configurations of **L** and **2** (**L′-Al** complex), DFT calculations were performed using **Gaussian-09** software over a Red Hat Linux IBM cluster. Molecular level interactions between **L** and **2** have been studied using density functional theory (DFT) with the **B3LYP/6-31G (d,p)** functional model and basis set.

From theoretical calculation it is reflected that both the HOMO and LUMO of **L′-Al** complex are more stabilized than **L** (Fig. 5). From the energy optimization of HOMO and LUMO of **L′-Al** complex, it could be easily pointed out that the more electronic charge density in HOMO over the rhodamine unit is pulled towards the nitro-benzene unit in the LUMO as usual. In case of **L** the electron density mainly resides on the half of the xanthene moiety and some electron density on the C=O moiety.
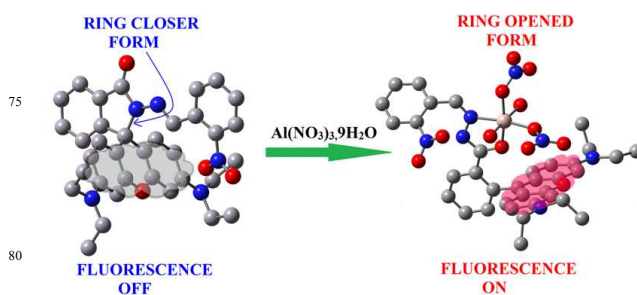
Scheme 2 Proposed mechanism of fluorescence enhancement of receptor (**L**) in presence of Al^{3+} ions.
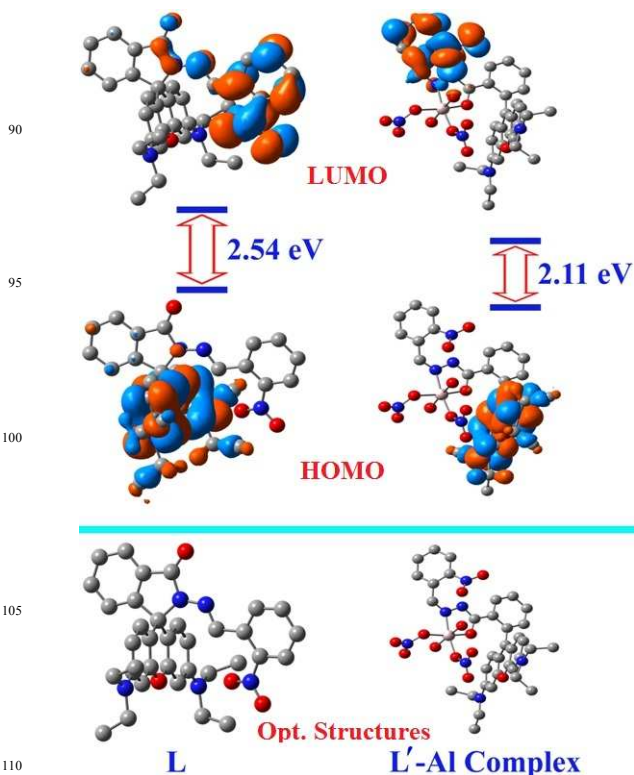
Fig. 5 Optimized structures and HOMO - LUMO's of **L** and **L′-Al** species (H atoms are omitted for clarity).

The UV spectra computed from TDDFT calculations in water show two important peaks in the range of 250-400 nm. For **L**, the band around 302.07 nm is dominated by the HOMO-3 → LUMO+1 and HOMO-9 → LUMO excitation, and the band around 312.35 nm is dominated by the HOMO-10 → LUMO, HOMO-8 → LUMO, HOMO-3 → LUMO+1 transitions (Fig. S17†). The details of the vertical excitation energies, oscillator strengths, and salient transitions are shown in Table S5†. For **L′-Al** species the band around 512.39 nm is dominated by the HOMO →LUMO+1, HOMO → LUMO+2, HOMO → LUMO+3 HOMO-2 → LUMO transition while the band around 481.33 and 376.02 nm is mainly due to HOMO → LUMO+2 and HOMO → LUMO+1 transition respectively (Fig. S18†). The band around 337.64 nm is dominated by the HOMO-6 → LUMO, HOMO-3 → LUMO+1, HOMO-2 → LUMO+3 transitions as tabulated in Tables S6. Here, the calculated spectra of the complex are found to be compatible with the experimental ones.

Spectroscopic studies of L′-Al complex in presence of F⁻ ions

To explore the utility of the resulting complex, **2**, the advantage of the fact of reversibility of ring-opening of spirolactam form was taken into consideration. Here the rupture of the **L′-Al** species to regenerate **L** and the subsequent change of optical properties of **L′-Al** system were studied by introducing several anions (F⁻, Cl⁻, Br⁻, I⁻, CN⁻, NO_3^-, ClO_4^-, $H_2PO_4^-$, HPO_4^{2-}, $H_2AsO_4^-$, $HAsO_4^{2-}$, AsO_3^{3-}, OAc⁻, SO_4^{2-}, $S_2O_3^{2-}$, S²⁻, SCN⁻ and PO_4^{3-}). In this study, the significant fluorescence quenching of **L′-Al** system due to regeneration of **L** was observed selectively in presence of F⁻ ions only (Fig. 6). This fact is in support of detection of fluoride ion using **L′-Al** system in presence of several competitive anions. Here, the strong interaction of hard-Al^{3+} ion and hard F⁻ ion possibly facilitates the breaking of **L′-Al** complex in support of quenching phenomenon through lowering of fluorescence intensity at 590 nm. Hence the fluorescence "*ON-OFF*" switching property of **L′-Al** complex could be used for detection of F⁻ ion in physiological conditions (1 mM HEPES buffer, pH 7.4) at 25°C (Fig. 7). Here, the intensities of the fluorescence were recorded after 10 min of addition of fluoride anion as it was then remained constant.
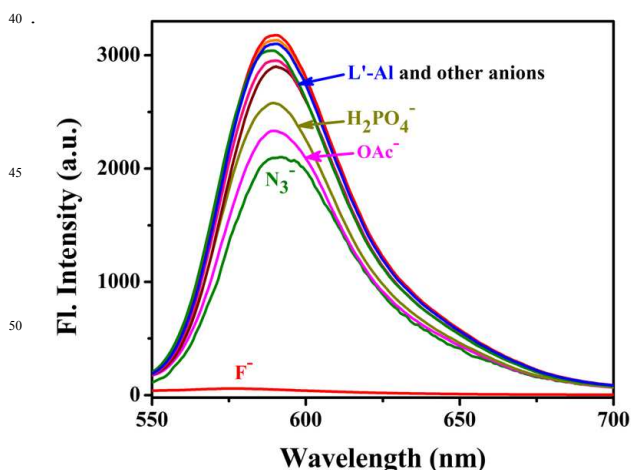
Fig. 6 Anion selectivity of **L′-Al complex** (10 μM) in presence of different anions in HEPES buffer (1 mM, pH 7.4; 25% EtOH) at λ$_{em}$= 590 nm at 25 °C.

Biological studies of L

To examine the utility of the probe in biological systems, it was applied to human cervical cancer HeLa cell and breast cancer cell MCF-7. MTT assay data indicates that the probe is not much cytotoxic with the IC$_{50}$ values of 46.4±0.7 μM in HeLa and > 50μM in MCF-7 cells respectively (Fig. S21 and S23†). Thus this probe can be applied for intracellular Al^{3+} ions detection since on complexation with Al^{3+} ions, the probe exhibit intense red fluorescence while itself is very weakly fluorescent.
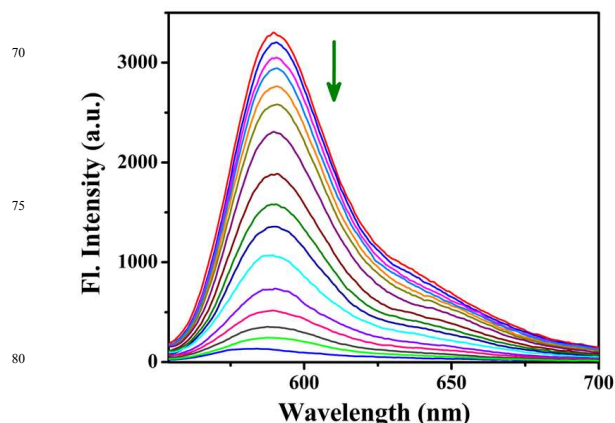
Fig. 7 Fluorescence titration spectra of **L′-Al** complex (10 μM) upon continuous addition of sodium fluoride (up to 30μM) in HEPES buffer (1 mM, pH 7.4; 25% EtOH) at 25°C (λ$_{ex}$ = 525 nm).

To study this possibility **L**, Al^{3+} and F⁻ ions were allowed to uptake by the cells of interest by incubation and the images of the cells were recorded by the fluorescence microscopy following excitation at 530 nm. After incubation with **L** (10 μM) for 30 min, the cells displayed insignificant fluorescence. However, cells exhibited intensive red fluorescence when exogenous Al^{3+} ions were introduced into the cell *via* incubation with Al(NO₃)₃ (Fig. 8 and S20, S22†). The fluorescence responses of **L** with various concentrations of added Al^{3+} ions are clearly evident from the cellular imaging.
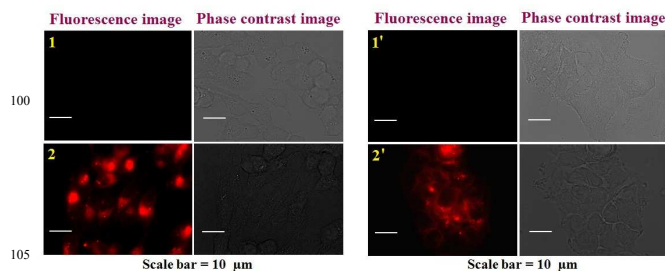
Fig. 8 Fluorescence image of HeLa cells (1, 2) and MCF-7 cells (1′, 2′) after incubation with **L** in presence of Al^{3+} ions (1, 1′) 0 μM, (2, 2′) 10 μM respectively at 37 °C following the excitation at 530 nm.

Moreover, the intense red fluorescence was deeply suppressed by scavenging Al^{3+} ions from the cell with the addition of NaF (Fig. 9 and S24†). This experiment proves that the binding of Al^{3+} ions with this chemosensor, **L**, is readily reversible inside the cellular environment. These results indicate that the probe has a huge potentiality for both *in vitro* and *in vivo*

application as Al³⁺ ions sensor as well as imaging in different ways as same manner for live cell imaging.
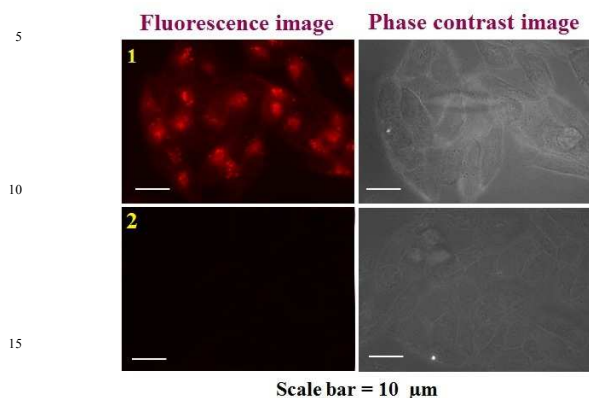
Fig. 9 Fluorescence image of HeLa cells after incubation with 10 μM **L′-Al** complex (1) followed by 50 μM of NaF (2) for 30 min at 37°C and the samples were excited at λ= 530 nm.

Conclusions

A new rhodamine based structurally characterised non-fluorescent Schiff base (**L**) selectively detects Al³⁺ ions upto 60.37 nm over other competitive ions through chelation enhanced fluorescence (CHEF) process in HEPES buffer (1 mM, pH 7.4; EtOH / water: 1/3, v/v) at 25 °C. The resulting fluorescent aluminium(III) complex (**L′-Al**) (**2**) was also isolated in pure form and characterised by detailed spectroscopic and physico-chemical tools. The remarkable quenching of fluorescence due to the addition of fluoride ions to complex **2**, enables the F⁻ ions detection as this optical change was not affected by other competitive anions in HEPES buffer (1 mM, pH 7.4; EtOH / water: 1/3, v/v) at 25 °C. As a result of this observation it may be concluded that the monitoring system is virtually real-time and stable, and the sensor **L** was recycled during the detection of fluoride anions. The same fact including the reversibility by selective addition of fluoride ion has also been observed in similar structural moiety with *ortho* methoxy group in place of nitro group.[47] It is also noteworthy to mention that the probes having the structural similarities of same substituents (methoxy and nitro groups) in the *para* position to the *benzylidene-hydrazido* unit behaved as Hg²⁺ ion selective sensors, perhaps the steric hindrance of the *ortho* substituents plays a key role to hinder the heavy metal ions (like Hg²⁺ ion) than the light metal ions (like Al³⁺ ion).[48] The experimental findings have also been supported by the theoretical (DFT) calculations. Moreover, the non-cytotoxic Al³⁺ ion selective **L** and the F⁻ ion selective complex **2** are highly potential biomarkers as these can easily recognize the intercellular distribution of respective ions in living cells under fluorescence microscope.

Acknowledgments

Notes and references

ᵃDepartment of Chemistry, The University of Burdwan, Golapbag, Burdwan 713104, India. E-mail: pabitracc@yahoo.com
ᵇDepartment of Inorganic and Physical Chemistry, Indian Institute of Science, Bangalore, 560012, India
† Electronic Supplementary Information (ESI) available: [Materials and physical methods, *general procedures*, tables, schemes, figures, characterization data, and some spectra], See *DOI: 10.1039/b000000x/*
‡ CCDC no for **L** is 997189.
Corresponding Author
* E-mail: pabitracc@yahoo.com. Tel: +91-342-2558554 extn. 424. Fax: +91-342-2530452.

1 M.G. Sont, S.M. White, W.G. Flamm and G.A. Burdock, *Regul. Toxicol. Pharm.*, 2001, **33**, 66.
2 (a) Z. Guo, S. Park, J. Yoon and I. Shin, *Chem. Soc. Rev.,* 2014, **43,** 16; (b) B. Sen, M. Mukherjee, S. Pal, S.K. Mondal, M.S. Hundal, A.R. Khuda-Bukhsh, and P. Chattopadhyay, *RSC Advances*, 2014, **3**, 19978; (c) M. Mukherjee, B. Sen, S. Pal, M. S. Hundal, S.K. Mandal, A.R. Khuda-Bukhsh and P. Chattopadhyay, *RSC Advances*, 2013, **3**, 19978; (d) C.R. Lohani, J.M. Kim, S.Y. Chung, J. Yoon and K.H. Lee, *Analyst*, 2010, **135**, 2079; (e) H.N. Kim, M.H. Lee, H.J. Kim, J.S. Kim and J. Yoon, *Chem. Soc. Rev.*, 2008, **37**, 1465.
3 W. Shi and H. Ma, *Chem. Commun.*, 2012, **48**, 8732.
4 Y. Yang, Q. Zhao, W. Feng and F. Li, *Chem. Rev.*, 2013, **113**, 192.
5 Y. Yang, S.K. Seidlits, M.M. Adams, V.M. Lynch, C.E. Schmidt, E.V. Anslyn and J.B. Shear, *J. Am. Chem. Soc.*, 2010, **132**, 13114.
6 N.W. Bavlor, W. Egan, P. Richman, *Vaccine* **2002**, **20**, S18.
7 W.S. Miller, L. Zhuang, J. Bottema, A.J. Wittebrood, P. De Smet, A. Haszler and A. Vieregge, *Mater. Sci. Eng: A*, 2000, **280**, 37.
8 R.E. Doherty, *Environ. Forensics*, 2000, **1**, 83.
9 G. Ciardelli and N. Ranieri, *Water Res.*, 2001, **35**, 567.
10 A Public Health Analysis of Dietary Aluminium, ed. S. Humphreys, P.M. Bolger, P.F. Zatta and A.C. Alfrey, World Scientific, Singapore, 1997, *pp*. 226.
11 R. Flarend, T. Bin, D. Elmore and S.L. Hem, *Food and Chemical Toxicology*, 2001, **39**, 163.
12 L. Yang, *Ann. Bot.*, 2006, **97**, 579.
13 L.V. Kochian and O.A. Hoekenga, *Annu. Rev. Plant Biol.*, 2004, **55**, 459.
14 D.P. Perl and A.R. Brody, *Science*, 1980, **208**, 297.
15 D.P. Perl, D.C. Gajdusek, R.M. Garruto and R.T. Yanagihara, C.J. Gibbs, *Science*, 1982, **217**, 1053.
16 E.H. Jeffery, K. Abreo, E. Burgess, J. Cannata and J.L. Greger, *J. Toxicol. Env. Health*, 1996, **48**, 649.
17 A. Becaria, A. Campbell and S. C. Bondy, *Toxicol. Ind. Health*, 2002, **18**, 309.
18 J.J. Spinelli, P.A. Demers, N.D. Le, M.D. Friesen, M.F. Lorenzi, R. Fang and R.P. Gallagher, *Cancer Cause Control*, 2006, **17**, 939.
19 K. Soroka, R.S. Vithanage, D.A. Phillips, B. Walker and P.K. Dasgupta, *Anal. Chem.*, 1987, **59**, 629.
20 P.D. Beer and P.A. Gale, *Angew. Chem. Int. Ed.*, 2001, **40**, 486.
21 R. Martinez-Manez and F. Sancenon, *Chem. Rev.*, 2003, **103**, 4419.
22 S. Kubik, *Chem. Soc. Rev.*, 2010, **39**, 3648.
23 T. Gunnlaugsson, M. Glynn, G.M. Tocci, P.E. Kruger and F.M. Pfeffer, *Coord. Chem. Rev.*, 2006, **250**, 3094.
24 J.L. Sessler and J.M. Davis, *Acc. Chem. Res.*, 2001, **34**, 989.
25 (a) E. Bianchi, K. Bowma-James and E. García-España, Eds. Supramolecular Chemistry of Anions; Wiley-VCH: New York, 1997; (b) P.A. Gale, *Acc. Chem. Res.* 2006, **39**, 465; (c) P. A. Gale, S. E. Garcia-Garrido and J. Garric, *Chem. Soc. Rev.*, 2008, **37**, 151; (d) A.F. Li, J.H. Wang, F. Wang and Y.B. Jiang, *Chem. Soc. Rev.*, 2010, **39**, 3729.
26 (a) R.H. Dreisbuch, Handbook of Poisoning; Lange Medical Publishers: Los Altos, CA, 1980; (b) K.L. Kirk, Biochemistry of the

Halogens and Inorganic Halides; Plenum Press: New York, 1991, *pp* 58; (c) M. Kleerekoper, *Endocrinol. Metab. Clin. North Am.*, 1998, **27**, 441.

27 M. Kleerekoper, *Endocrinology and Metabolism Clinics of North America.*, 1998, **27**, 441.

28 D. Browne, H. Whelton and D. O'Mullane, *Journal of Dentistry*, 2005, **33**, 177.

29 R.P. Schwarzenbach, B.I. Escher, F. Kathrin, T.B. Hofstetter, C.A. Johnson, U. V. Gunten and B. Wehrli, *Science.*, 2006, **313**, 1072.

30 S. Jagtap, M.K. Yenkie, N. Labhsetwar and S. Rayalu, *Chem. Rev.*, 2012, **112**, 2454.

31 (a) S. Samanta, S. Goswami, Md.N. Hoque, A. Ramesh and G. Das, *Chem. Commun.*, 2014, **50**, 11833; (b) E. Furia, T. Marino and N. Russo, *Dalton Trans.*, 2014, **43**, 7269; (c) Y. Fu, X.J. Jiang, Y.Y. Zhu, B.J. Zhou, S.Q. Zang, M.S. Tang, H.Y. Zhang and T.C.W. Mak, *Dalton Trans.*, 2014, **43**, 12624; (d) W.H. Ding, W. Cao, X.J. Zheng, W.J. Ding, J.P. Qiao and L.P. Jin, *Dalton Trans.*, 2014, **43**, 6429; (e) Neeraj, A. Kumar, V. Kumar, R. Prajapati, S.K. Asthana, K.K. Upadhyay and J. Zhao, *Dalton Trans.*, 2014, **43**, 5831 and references therein; (f) M. Mukherjee, S. Pal, S. Lohar, B. Sen, S. Banerjee, S. Banerjee and P. Chattopadhyay, *Analyst*, 2014, **139**, 4828 and references therein; (g) T. Mistri, R. Alam, R. Bhowmick, S.K. Mandal, M. Dolai, A.R. Khuda-Bukhsh and M. Ali, *Analyst*, 2014, DOI: 10.1039/C3AN02255B; (h) B. Sen, S. Pal, S. Lohar, M. Mukherjee, S.K. Mandal, A.R. Khuda-Bukhsh and P. Chattopadhyay, *RSC Advances*, 2014, **4**, 21471; (i) A. Dhara, A. Jana, S. Konar, S.K. Ghatak, S. Ray, K. Das, A. Bandyopadhyay, N. Guchhait and S.K. Kar, *Tetrahedron Lett.*, 2013, **54**, 3630; (j) S. Das, M. Dutta and D. Das, *Anal. Methods*, 2013, **5**, 6262 and references therein; (k) S. Sen, T. Mukherjee, B. Chattopadhyay, A. Moirangthem, A. Basu, J. Marek and P. Chattopadhyay, *Analyst*, 2012, **137**, 3975.

32 (a) K. Dhanunjayarao, V. Mukundam and K. Venkatasubbaiah, *J. Mater. Chem. C*, 2014, *DOI: 10.1039/c4tc01711k* and references therein; (b) H. Khanmohammadi and K. Rezaeian, *RSC Adv.*, 2014, **4**, 1032; (c) S. Madhu and M. Ravikanth, *Inorg. Chem.*, 2014, **53**, 1646; (d) C. Saravanan, S. Easwaramoorthi, C.Y. Hsiow, K. Wang, M. Hayashi and L. Wang, *Org. Lett.*, 2014, **16**, 354; (e) Q. Song, A. Bamesberger, L. Yang, H. Houtwed and H. Cao, *Analyst*, 2014, **139**, 3588; (f) J.S. Chen, P.W. Zhou, G.Y. Li, T.S. Chu and G.Z. He, *J. Phys. Chem. B*, 2013, **117**, 5212; (g) P. Das, A.K. Mandal, M.K. Kesharwani, E. Suresh, B. Ganguly and A. Das, *Chem. Commun.*, 2011, **47**, 4398; (h) L. Gai, H. Chen, B. Zou, H. Lu, G. Lai, Z. Li and Z. Shen, *Chem. Commun.*, 2012, **48**, 10721; (i) X. Cao, W. Lin, Q. Yu and J. Wang, *Org. Lett.*, 2011, **13**, 6098; (j) R. Hu, J. Feng, S. Wang, S. Li, Y. Li and G. Yang, *Angew. Chem., Int. Ed.*, 2010, **49**, 4915; (k) E. Galbraith and T.D. James, *Chem. Soc. Rev.*, 2010, **39**, 3831; (l) S.Y. Kim, J. Park, M. Koh, S.B. Park and J.I. Hong, *Chem. Commun.*, 2009, **45**, 4735.

33 (a) Y.H. Zhao, X. Zeng, L. Mu, J. Li, C. Redshaw and G.Wei, *Sensors and Actuators B*, http://dx.doi.org/doi:10.1016/j.snb.2014.07.048; (b) S.B. Maity and P.K. Bharadwaj, *Inorg. Chem.*, 2013, **52**, 1161; (c) A. Kumar, V. Kumar and K.K. Upadhyay, *Analyst*, 2013, **138**, 1891; (d) Y. Bao, B. Liu, F. Du, J. Tian, H. Wang and R. Bai, *Mater. Chem.*, 2012, **22**, 5291.

34 B. Sen, M. Mukherjee, S. Pal, K. Dhara, S.K. Mandal, A.R. Khuda-Bukhsh and P. Chattopadhyay, *RSC Advances*, 2014, **4**, 14919.

35 A. Altomare, G. Cascarano, C. Giacovazzo and A. Guagliardi, *J. Appl. Crystallogr.*, 1993, **26**, 343.

36 G.M. Sheldrick, *Acta Cryst A*, 2008, **64**, 112.

37 L.J. Farrugia, *J. Appl. Cryst.*, 1999, **32**, 837.

38 (a) M. Cossi, N. Rega, G. Scalmani, V. Barone, *J. Comput. Chem.*, 2003, **24**, 669; (b) M. Cossi, V. Barone, *J. Chem. Phys.*, 2001, **115**, 4708; (c) V. Barone, M. Cossi, *J. Phys. Chem. A*, 1998, **102**, 1995.

39 M.E. Casida, C. Jamorski, K.C. Casida, D. R. Salahub. *J. Chem. Phys.*, 1998, **108**, 4439.

40 N.M. O'Boyle, A. L. Tenderholt, K.M. Langner, *J. Comput. Chem.*, 2008, **29**, 839.

41 (a) J. Ratha, K.A. Majumdar, S.K. Mandal, R. Bera, C. Sarkar, B. Saha, C. Mandal, K.D. Saha, R. Bhadra, *Mol. Cell Biochem.*, 2006, **290**, 113; (b) S. Banerjee, P. Prasad, A. Hussain, I. Khan, P. Kondaiah and A.R. Chakravarty, *Chem. Commun.*, 2012, **48**, 7702;

(c) S. Banerjee, A. Dixit, R.N. Shridharan, A.A. Karande and A.R. Chakravarty, *Chem. Comm.*, 2014, **50**, 5590.

42 (a) X. Chen, T. Pradhan, F. Wang, J.S. Kim, and J. Yoon, *Chem. Rev.*, 2012, **112**, 1910; (b) S. Pal, B. Sen, M. Mukherjee, K. Dhara, S.K. Mandal, E. Zangrando, A.R. Khuda-Bukhsh, and P. Chattopadhyay, *Analyst*, 2014, **139**, 1628; (c) B. Sen, M. Mukherjee, S. Pal, K. Dhara, S. K. Mandal, A. R. Khuda-Bukhsh and P. Chattopadhyay, *RSC Advances*, 2014, **4**, 14919.

43 A. Mallick, B. Haldar, and N. Chattopadhyay, *Photochem. Photobiol.*, 2005, **78**, 215.

44 H.A. Benesi and J.H. Hildebrand, *J. Am. Chem. Soc.*, 1949, **71**, 2703.

45 A. Hakonen, *Anal. Chem.*, 2009, **81,** 4555.

46 N.J. Turro, Modern Molecular Photochemistry; Benjamin/ Cummings Publishing Co., Inc.: Menlo Park, CA, 1978.

47 B. Sen, S. Pal, S. Banerjee, S. Lohar and P. Chattopadhyay, *Eur. J. Inorg. Chem.*, 2015, DOI: 10.1002/ejic.201403091.

48 S. Pal, B. Sen, M. Mukherjee, K. Dhara, E. Zangrando, S.K. Mandal, A.R. Khuda-Bukhsh and P. Chattopadhyay, *Analyst*, 2014, **139**, 1628.